Nuclear Instruments and Methods in Physics Research A327 (1993) 193–198
North-Holland

NUCLEAR INSTRUMENTS & METHODS IN PHYSICS RESEARCH
Section A

Liquid krypton electromagnetic calorimeter

V.M. Aulchenko, A.D. Bukin, S.G. Klimenko, G.M. Kolachev, L.A. Leontiev, A.L. Maslennikov, A.P. Onuchin, V.S. Panin, S.V. Peleganchuk, S.G. Pivovarov, V.A. Rodyakin, V.A. Tayursky, Yu.A. Tikhonov and V.I. Yurchenko

Budker Institute of Nuclear Physics, Novosibirsk, Russian Federation

F. Lanni, G. Lo Bianco, B. Maggi, F. Palombo and A. Sala

Dipartimento di Fisica dell'Universita' and Sezione INFN, Milan, Italy

P. Cantoni, P.L. Frabetti and L. Stagni

Dipartimento di Fisica dell'Universita' and Sezione INFN, Bologna, Italy

P.F. Manfredi, V. Re and V. Speziali

Dipartimento di Elettronica Universita' di Pavia and Sezione INFN, Milan, Italy

A calorimeter using 30 tons of liquid krypton for the KEDR detector is being constructed. The main effects which determine the energy and space resolution have been studied. An energy resolution of 1.7% at 1.2 GeV was obtained with the prototype. A space resolution of 0.4 mm for relativistic particles has been reached with the prototype.

1. Introduction

An electromagnetic calorimeter employing 30 tons of liquid krypton (LKr) [1,2] was suggested for the KEDR experiment in the energy region of Upsilon-mesons. Considerable effort was devoted to study the main factors determining the energy and space resolution and the technical design of the LKr calorimeter was developed [3–8]. The manufacture of the main parts of calorimeter is finishing now and the mounting is being prepared.

Use of liquid krypton for the calorimeter is attractive due to the possibility of obtaining good energy resolution (comparable with that of NaI, CsI and BGO calorimeters) and better space resolution for photons in comparison with crystal calorimeters. This is due to the possibility of measuring the photon conversion point in contrast to the crystal detectors where the photon coordinates are determined by the shower center-of-gravity.

Moreover, longitudinal segmentation of the LKr calorimeter provides important information for particle identification by dE/dx as well as e/π separation.

2. Space characteristics of showers in LKr

Using Monte Carlo simulation we have calculated [6] the main features of showers produced by photons in LKr. A part of these calculations was made taking into account the magnetic field (H) of 1.8 T directed perpendicularly to the shower axis.

In the table 1 we present the average energy deposition W and its fluctuations σ_w/E in LKr layer with a

Table 1
Energy deposition W/E and its fluctuations obtained in Monte Carlo simulation. Thickness of LKr layer is 70 cm

E [GeV]	0.1	0.2	0.5	1.0	2.0	5.0
W/E [%]	98.6	98.4	98.0	97.3	96.0	95.2
σ_w/E [%]	0.4	0.5	0.8	1.1	1.4	2.3

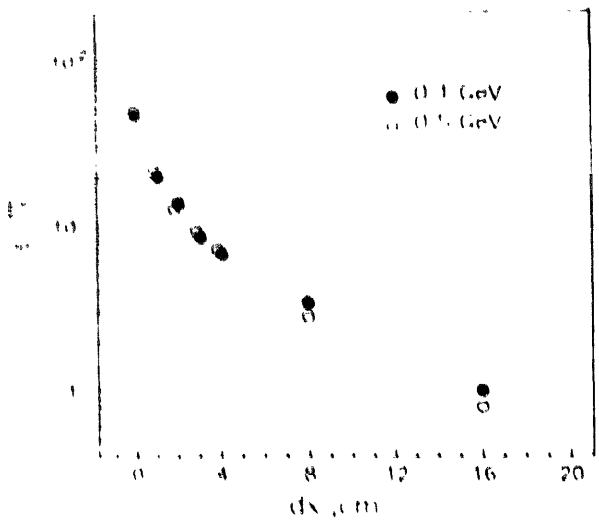

Fig. 1. Monte Carlo simulation. The fraction of the photon energy going to the neighboring block versus the distance of the photon from the boundary between the blocks for 0.1 and 0.5 GeV photons.

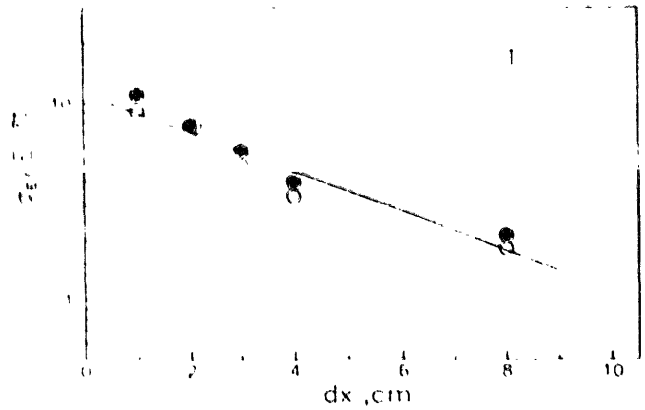

Fig. 2. Monte Carlo simulation. Contribution to the energy resolution of the transverse leakage versus the distance to the block boundary. Black circles – $E_\gamma = 0.1$ GeV, open circles – $E_\gamma = 0.5$ GeV (fit by hand).

thickness of 70 cm ($15.1 X_0$). The quantity σ_w was calculated as FWHM/2.36.

The data concerning energy fraction (K_B), reflected back from LKr, as a function of the energy of photons, falling normally to the LKr surface, are shown in table 2.

In figs. 1 and 2 data are presented for the case, when a photon falls on the calorimeter at some distance from the boundary between two large blocks ($H = 0$). The thickness of LKr is 70 cm.

Fig. 3 depicts the transverse distribution of the shower energy in first three layers from the beginning of the shower ($H = 0$). Each layer has a thickness of 4 cm. The events have been selected with the conversion in the first layer.

Data concerning the accuracy of the photon conversion point reconstruction are presented in table 3. The geometry is shown in fig. 4. The depth of LKr gap is $\Delta z = 4$ cm. The magnetic field was directed along the x-axis. Two neighboring layers were used for the coordinates determination. The first one is the layer containing the conversion point. The values σ_1 and σ_2 are the rms fluctuations of the shower center-of-gravity in the first and the second layers respectively. Letter A

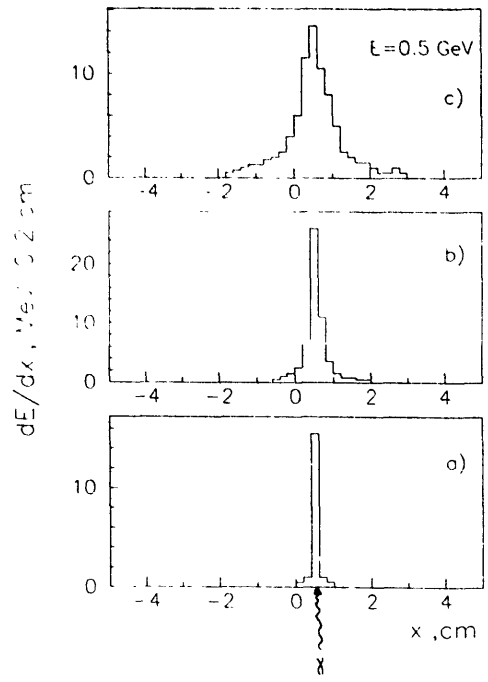

Fig. 3. Monte Carlo simulation. The transverse distribution of the energy released in the first three layers for the photon energy of 0.5 GeV.

Table 2
Calculated fraction of photon energy reflecting back from LKr

E [GeV]		0.05	0.1	0.2	0.5	1.0	5.0
K_B [%]	$H = 0$	0.76	0.53	0.35	0.27	0.22	0.09
	$H = 1.8$ T	1.2	0.87	0.61	0.43	0.33	0.18

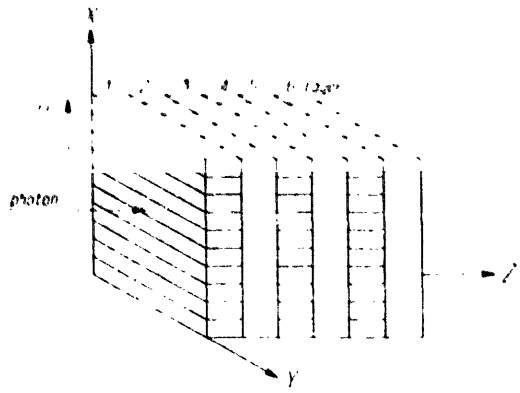

Fig. 4. LKr layer segmentation for the determination of the photon conversion point.

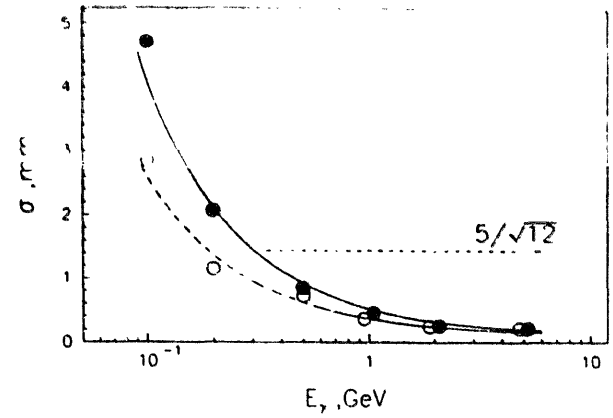

Fig. 5. Monte Carlo simulation. Average (of z and ϕ) space resolution. Black circles – magnetic field of 1.8 T, open circles – without magnetic field.

denotes a case when the conversion occurred in an odd layer, B in an even one.

The effective fluctuation (σ), shown in fig. 5 was defined for the case with magnetic field of 1.8 T as:

$$\sigma = \tfrac{1}{2}\left[\left(\sigma_1^{\mathrm{A}}\right)^2 + \left(\sigma_2^{\mathrm{A}}\right)^2 + \left(\sigma_1^{\mathrm{B}}\right)^2 + \left(\sigma_2^{\mathrm{B}}\right)^2\right]^{1/2},$$

and without magnetic field as $\sigma = [(\sigma_1^2 + \sigma_2^2)/2]^{1/2}$.

3. LKr calorimeter of the KEDR detector

The lay-out of the LKr calorimeter [8] is shown in fig. 6. The inner radius is 75 cm, the thickness is 68 cm ($15X_0$), the length is about 3 m. To diminish the amount of LKr required, special aluminium rings will be placed inside the cold barrel close to flanges and outer surface of the cylinder so that the LKr thickness should be the same in any direction for particles originating from the interaction point. It saves about 5 tons of Kr, and the amount necessary is 30 ton.

The entrance wall of the cryostat contains 1 mm of stainless steel and 14 mm of aluminium. The electrodes are made of fiber glass with thickness 0.5 mm of G10 and covered with 2×18 μm of copper foil. The inter-electrode gap is 20 mm.

The signal is read out from high voltage electrodes, divided into rectangular pads, forming towers, oriented to the interaction point. The entrance size of the towers is 10×10 cm^2. In the radial direction all the towers are divided into three sections. The grounded electrodes of the first section (30 cm thick) are divided into strips of about 5 mm width. The strips orientation is along the beam line direction (z-axis) in four electrodes and along the orthogonal direction (ϕ) in the other four. The strips are used for the photon coordinates measurement as well as for $\mathrm{d}E/\mathrm{d}x$ measurements. The width of the towers and z-strips is increased along z-axis providing the uniform resolution in the polar angle.

The total number of electronics channels is 7.2×10^3, 2.4×10^3 of them are connected to the towers, the others to the strips.

4. Energy resolution

Showers produced in LKr were simulated by a Monte Carlo method for the real structure of the calorimeter in the presence of a magnetic field of 1.8

Table 3
Calculated fluctuations of center of gravity σ [mm]. Transverse segmentation of layers of LKr is 2 mm

E [GeV]	$H = 1.8$ T, case A		$H = 1.8$ T, case B		$H = 0$	
	σ_1^{A}	σ_2^{A}	σ_1^{B}	σ_2^{B}	σ_1	σ_2
0.1	0.55	8.5	0.55	4.0	0.5	4.0
0.2	0.35	3.6	0.35	2.0	0.3	1.6
0.5	0.22	1.3	0.24	1.0	0.17	1.0
1.0	0.12	0.7	0.14	0.55	0.13	0.5
2.0	0.10	0.35	0.10	0.35	0.06	0.35
5.0	0.06	0.30	0.09	0.30	0.06	0.30

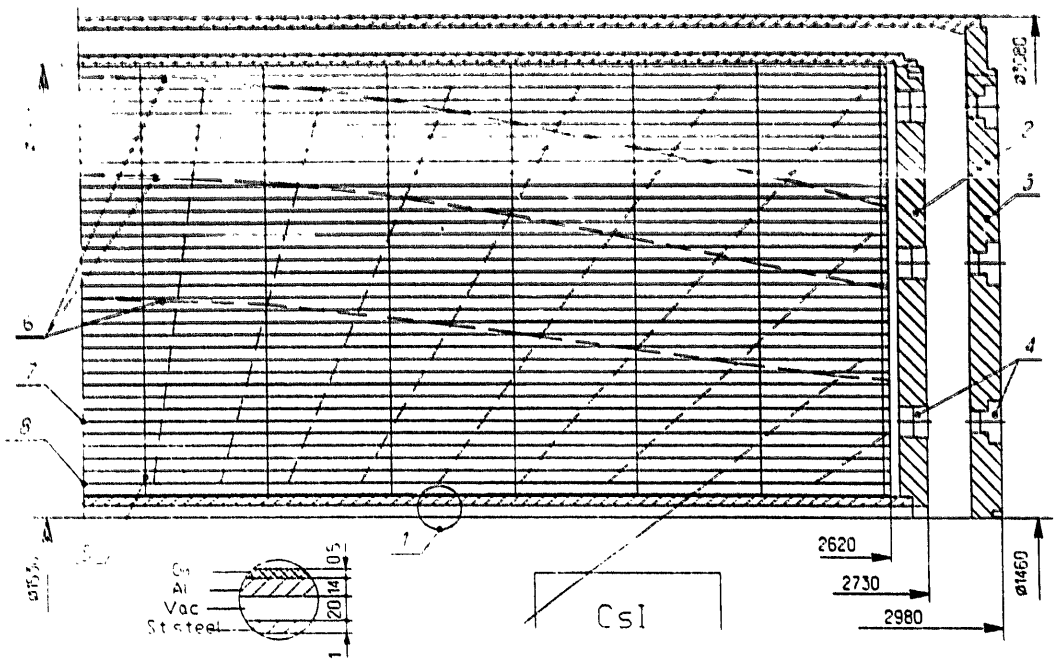

Fig. 6. The lay out of the LKr calorimeter. 1 – entrance wall, 2 – cold flange, 3 – warm flange, 4 – multipin connectors, 5 – spacers, 6 – lines of equal thickness, 7 – strip electrode, 8 – high voltage (tower) electrode.

T, taking into account the signal processing. The calculation data of the main effects contributing to the energy resolution in the energy region 100-1000 MeV are listed below.

1) The energy leakage in the longitudinal direction (L) and sampling fluctuations (S). They ($L + S$) are fitted together by

$$(\sigma/E) = 0.8\% + 0.3\%E^{1/2}\ [\mathrm{GeV}].$$

2) The energy leakage in the transverse direction (T). The value of this effect depends on the transverse size of the block (number of towers) and on the photon distance to the boundary of the block; the results are shown in figs. 1, 2.

3) Electronics noise (N) and radioactivity (R). The method of the radioactive noise (R) calculation was described elsewhere [8]. At the optimal time constant, $\tau = 1$ μs, the $R + N$ contribution is 0.85 Mev.

4) Geometric factor (G). This effect arises from the signal dependence of the charge distribution inside the gap. Its value decreases with the decreasing of the charge collection time (shaper time constant (τ)). But the electronics noise (N) is increased in this case; and the optimal value of τ is close to 1 μs, that corresponds to 5–10% fraction of the total charge collected.

In our calculation [4] of the geometric factor, carried out using the code UNIMOD [9], there was an error. A note about this was in ref. [8]. We have carried out a new calculation with high statistics, using the codes UNIMOD and GEANT and received the same result. It is interesting to note, that fluctuations of the ionization losses practically do not influence the geometric factor. It is determined by the fluctuations in development of shower. Thus, when the Landau fluctuations were put equal to zero, the value of G appeared to be the same within statistical errors.

The thickness of LKr giving contribution to the geometric factor approximately equals to the length of electron drift for the shaper time constant. For our case, a shaper time constant of 1 μs corresponds to the thickness of 2 mm.

Fig. 7 shows results of the calculation of the geometric factor as a function of energy for the RC–2CR

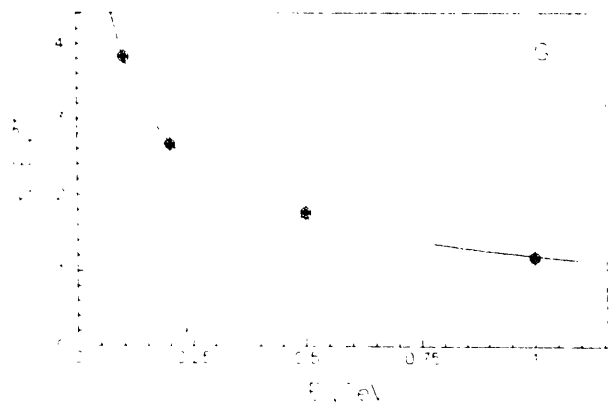

Fig. 7. Monte Carlo simulation. Contribution of the geometric effect to the energy resolution; shaper time constant/drift time = 0.1.

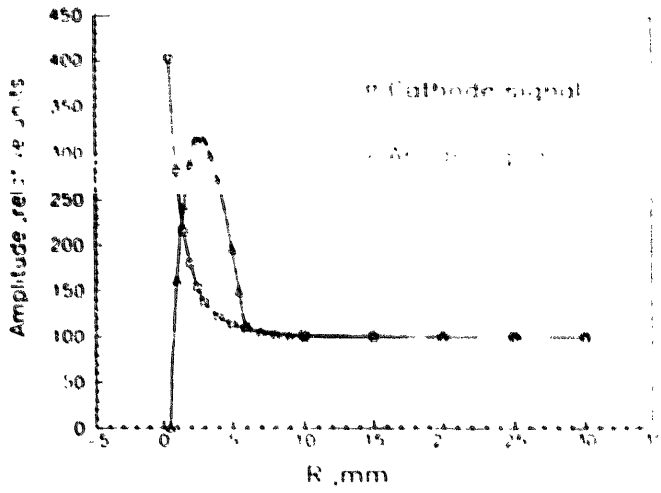

Fig. 8. Monte Carlo simulation. The pulse height versus the distance between the particle and the wire.

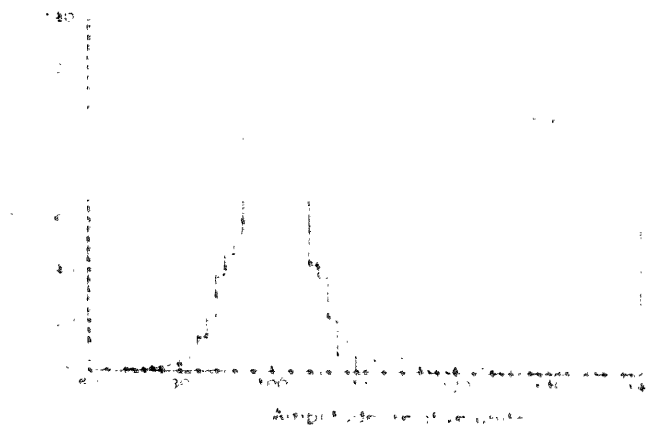

Fig. 9. Monte Carlo simulation. The amplitude spectra without a wire (solid) and with it (dashed).

shaper with $\tau = 1$ μs, drift time equals to 10 μs. The data on G are approximated by the dependence

$$(\sigma_E/E)_G = 1.2\% E^{-1/2} \quad [\text{GeV}].$$

This calculation was carried out in the assumption, that the absorption length of electrons in LKr is infinite. Naturally, taking into account of the finite absorption length diminishes the geometric factor, since this diminishes effective thickness, contributing to G. Now we are performing such calculations.

5) Algorithm of photon energy reconstruction. We have carried out a calculation of the energy resolution, accounting the effects discussed above, with 3 × 3 towers (30 cm × 30 cm), three layers were taken in longitudinal direction. The best resolution was obtained when the towers with maximum puls hights were sumed; the number of these towers depends on energy [4,5,8]. It can be approximated by

$$\sigma_E/E = 1.9\% E^{-1/2} \text{ [GeV]}.$$

6) Other effects.

a) Variations of gaps between electrodes (V).

This effect depends approximately linearly on the value of variation of gaps and as $\sqrt{E}$ on the energy. At $E = 0.1$ GeV this effect equals 1.7% for the 5% variance of gaps [3,4,8].

b) Electric field distortion in the gap (E).

The signal readout wires crossing the gaps distort the electric field. Fig. 8 gives the result of a Monte Carlo calculation of the signal pulse height. The calculation was performed for relativistic particles as a function of the distance from particle trajectory to wire. Two curves correspond to the cases of the cathode and anode readout. The pulse shaping is RC-2CR with $\tau = 1$ μs time constant. One can see, that noticeable distortion of amplitude takes place, if the distance of the particle trajectory to the wire is less than 5 mm.

Fig. 9 shows the result of a simulation of the amplitude spectrum for showers of 0.1 GeV photons, when in all gaps in longitudinal direction there is such a distortion of the field, as well as without such distortion. The photon flux is distributed uniformly over the area of 10 × 10 cm^2 (the size of tower), with the wire in the center. One can see the spectrum changed a little in the region of large amplitudes. But in this calculation the contributions of L, S, T, G, N, R effects were neglected. In table 4 the data on probability of an event appearing with a large amplitude are represented. The contributions of $L + S$ and E effects are presented. One can see, that for the given construction of the calorimeter, when the distance between the wires for signal readout is about 10 cm, the E effect is negligible.

There are a lot of other effects (inaccuracy of relative calibration of electronics channels, cross talk, instability of electronics and others). These effects should

Table 4
Calculated probability [%] of events appearing with an amplitude of more than average by a value Δ

	$E_\gamma = 0.1$ [GeV]			$E_\gamma = 1$ [GeV]		
Δ [%] →	6	10	15	2	4	6
$L + S$	10	7	5	16	9	6
E (cathode)	8	1.0	0.5	9	2	1
E (anode)	9	2.5	1.5	11	3	2

be controlled to diminish their contribution to the resolution. There will also be a problem of the abso'ute calibration of the energy.

5. Spatial resolution

The spatial resolution for photons is determined by fluctuations of the shower center-of-gravity and by the measurement precision of the ionization position. The fluctuations of the shower were discussed in the second section (table 3 and fig. 5).

The measurement precision of the ionization position has some peculiarity depending on many parameters [3]. If a charge of one sign only is measured at the anode, the coordinate is determined by the strips width s. When the integration time is more than the total drift time of electrons in the gap the charge distribution at the cathodes is less peaked compared to the one at the anode and the accuracy of the center of gravity is determined by the electronics noise and the value of $\sigma = 0.2$ mm can be easily achieved for relativistic particles [3]. When only a small fraction of the charge is collected the distribution of the charge on the cathode is very narrow and the resolution is about $s/\sqrt{12}$.

6. Particle identification

Pulse height measurements from the strips can be used for charge particle identification by dE/dx method. The result of calculations for five gaps of LKr shows the possibility of π–K separation at the level over 2σ up to the momentum of 1 GeV/c [6].

7. Prototype results

For the experimental study of the LKr technique we have built two prototypes: Prototype-7 (7 kg of LKr) and Prototype-400 (400 kg of LKr). The first one aimed at the measurement of the space resolution for the charged particles. In the experiment with cosmic particles we obtained space resolution $\sigma = 3$ mm in anode readout mode and $\sigma = 0.4$ mm with the cathode readout. The details of this experiment were described elsewhere [3].

The experiment with Prototype-400 was devoted to the energy resolution measurement [3]. The energy resolution of 1.7% at 1.2 GeV and 5.7% at 0.13 GeV was obtained [3]. The energy resolution obtained is comparable with that of CLEO-II and KEDR CsI calorimeter prototypes and L3 BGO calorimeter prototype.

We also performed the experiment with Prototype-400 signal reading out both from cathodes and anodes [6–8]. The structure of electrodes contained towers and strips. The obtained energy resolution was about the same, as in the experiment [3].

References

[1] V.V. Anashin et al., Proc. Int. Symp. on position Detect. in High Energy Physics, Dubna, 1988, eds. M.I. Zarubina and E.V. Ivashkevich (JINR) p. 58.
[2] V.M. Aulchenko et al., Proc. 24 Int. Conf. on High Energy Physics, Munich, 1988 (contrib. paper) eds. R. Kotthaus and J.H. Kuhn (Springer, Berlin).
[3] V.M. Aulchenko et al., Nucl. Instr. and Meth. A289 (1990) 468.
[4] V.M. Aulchenko et al., Proc. 5th Int. Conf. on Instr. for Coll. Beam Phys., Novosibirsk, 1990, ed. E.P. Solodov (World Scientific, Singapore) p. 299.
[5] V.M. Aulchenko et al., Conf. on Calorimetry in High Energy Physics, FNAL, 1990, Eds. F. Anderson, M. Derrich, H.E. Fisk, A. Para and C.M. Sazama (World Scientific) p. 233.
[6] V.M. Aulchenko et al., Experimental Apparatus for High Energy Particle Physics and Astrophysics, ed. P. Giusti et al. (World Scientific, 1991) p. 326.
[7] P. Cantoni et al., Nucl. Instr. and Meth. A315 (1992) 491.
[8] V.M. Aulchenko et al., Nucl. Instr. and Meth. A316 (1992) 8.
[9] A.D. Bukin et al., MC91, Workshop on Detector and Event Simulation in High Energy Physics, Amsterdam 1991, eds. Kors Bos and Bob van Eijk (NIKHEF) p. 79.